

Determination of Three-dimensional Structure and Residues of the Novel Tumor Suppressor AIMP3/p18 Required for the Interaction with ATM^{*[5]}

Received for publication, February 1, 2008, and in revised form, March 11, 2008. Published, JBC Papers in Press, March 14, 2008, DOI 10.1074/jbc.M800859200

Kyung-Jin Kim⁺¹, Min Chul Park^{S1}, So Jung Choi^S, Young Sun Oh^S, Eung-Chil Choi^S, Hyo Je Cho¹, Myung Hee Kim^{||}, Soo-Hyun Kim^{**}, Dong Wook Kim^{**}, Sunghoon Kim^{S2}, and Beom Sik Kang¹³

From the ⁺Pohang Accelerator Laboratory, Pohang University of Science and Technology, Pohang 790-784, Korea, the ^SCenter for Medicinal Protein Network and Systems Biology, College of Pharmacy, Seoul National University, Seoul 151-742, Korea, the ^{||}Korea Research Institute of Bioscience and Biotechnology, Daejeon 305-806, Korea, the ^{**}Division of Hematology, St. Mary's Hospital College of Medicine, The Catholic University of Korea, Seoul 150-713, Korea, and the ¹School of Life Science and Biotechnology, Kyungpook National University, Daegu 702-701, Korea

Although AIMP3/p18 is normally associated with the multi-tRNA synthetase complex via its specific interaction with methionyl-tRNA synthetase, it also works as a tumor suppressor by interacting with ATM, the upstream kinase of p53. To understand the molecular interactions of AIMP3 and the mechanisms involved, we determined the crystal structure of AIMP3 at 2.0-Å resolution and identified its potential sites of interaction with ATM. AIMP3 contains two distinct domains linked by a 7-amino acid (Lys⁵⁷–Ser⁶³) peptide, which contains a 3₁₀ helix. The 56-amino acid N-terminal domain consists of two helices into which three antiparallel β strands are inserted, and the 111-amino acid C-terminal domain contains a bundle of five helices (Thr⁶⁴–Tyr¹⁵²) followed by a coiled region (Pro¹⁵³–Leu¹⁶⁹). Structural analyses revealed homologous proteins such as yeast glutamyl-tRNA synthetase, Arc1p, EF1Bγ, and glutathione S-transferase and suggested two potential molecular binding sites. Moreover, mutations at the C-terminal putative binding site abolished the interaction between AIMP3 and ATM and the ability of AIMP3 to activate p53. Thus, this work identified the two potential molecular interaction sites of AIMP3 and determined the residues critical for its tumor-suppressive activity through the interaction with ATM.

Although aminoacyl-tRNA synthetases (ARSs)⁴ catalyze the ligation of specific amino acids to their cognate tRNAs, they are multifunctional proteins that are involved in the regulation of diverse signal pathways (1). Several ARSs of higher eukaryotes form an intriguing macromolecular protein complex with three non-enzymatic factors, designated AIMP3 (ARS-interacting multifunctional proteins), which are also multiply involved in various biological processes. Of these factors, AIMP1/p43 is secreted as a cytokine that functions in immune response (2, 3), angiogenesis (4), and wound-healing processes (5) and also as a hormone that regulates glucose metabolism (6). AIMP2/p38 has been shown to mediate transforming growth factor-β signaling for c-Myc down-regulation (7). AIMP3/p18 binds to the multi-ARS complex by specifically interacting with methionyl-tRNA synthetase (MRS) and is translocated to the nucleus to activate p53 through the interaction with kinases such as ATM (ataxia telangiectasia mutated) and ATR (ATM- and Rad3-related) in response to DNA damage (8) or oncogenic stress (9). To understand the multifunctionality and regulation of the components of the multi-ARS complex, it is important to determine the three-dimensional structures of the components as well as the whole complex. So far, only the three-dimensional structures of the partial domains of the complex-forming ARSs such as glutamylprolyl-tRNA synthetase (10, 11), aspartyl-tRNA synthetase (12), and AIMP1/p43 (13, 14) have been elucidated. Here, we report the crystal structure of full-length AIMP3 and the residues and location required for the interaction with ATM.

EXPERIMENTAL PROCEDURES

Cloning, Expression, and Purification of Human AIMP3—The cDNA encoding human AIMP3 was amplified by PCR and subcloned into pProEx-HTa (NdeI), a His₆ fusion expression vector containing a recombinant tobacco etch virus protease cleavage site and a site for NdeI. For the SeMet-substituted protein preparation, Thr⁴², Ile⁷⁰, and Lys⁹⁵ residues were replaced by methionine using site-directed mutagenesis because the N-terminal methionine residue was not sufficient

* This work was supported by the 21C Frontier Microbial Genomics and Application Center Program, Korea Science and Engineering Foundation Grant R17-2007-020-01000-0 from the Ministry of Science and Technology, and Basic Research Program Grant R21-2007-000-10041-0 from the Science and Engineering Foundation, Republic of Korea. The costs of publication of this article were defrayed in part by the payment of page charges. This article must therefore be hereby marked "advertisement" in accordance with 18 U.S.C. Section 1734 solely to indicate this fact.

[5] The on-line version of this article (available at <http://www.jbc.org>) contains supplemental Tables 1–3.

The atomic coordinates and structure factors (code 2UZ8) have been deposited in the Protein Data Bank, Research Collaboratory for Structural Bioinformatics, Rutgers University, New Brunswick, NJ (<http://www.rcsb.org/>).

¹ Both authors equally contributed to this work.

² To whom correspondence may be addressed: Seoul National University, Kwanak-ro 599, Kwanak-gu, Seoul 151-742, Korea. Tel.: 822-880-8180; Fax: 822-875-2621; E-mail: sungkim@snu.ac.kr.

³ To whom correspondence may be addressed: Kyungpook National University, Sankyong-dong 1370, Buk-gu, Daegu 702-701, Korea. Tel.: 82-53-950-6357; E-mail: bskang2@knu.ac.kr.

⁴ The abbreviations used are: ARS, aminoacyl-tRNA synthetase; MRS, methionyl-tRNA synthetase; ERS, glutamyl-tRNA synthetase; GST, glutathione S-transferase; CML, chronic myeloid leukemia.

for phasing in structural determination. To improve crystal quality, the C-terminal 5 residues (Tyr¹⁷⁰–His¹⁷⁴) were truncated because the residues are thought to be flexible based on secondary structure prediction. The resulting recombinant vectors, pP_{ROEX}-HTa:AIMP3, pP_{ROEX}-HTa:AIMP3(Δ C5), and SeMet-substituted AIMP3 (Δ C5,T42M/I70M/K96M), were transformed into the methionine auxotroph *Escherichia coli* strain B834 (Novagen).

Transformants were grown in an LB medium containing ampicillin at 37 °C until reaching an A₆₀₀ between 0.6 and 0.8. After induction with 1.0 mM isopropyl 1-thio- β -D-galactopyranoside, cultures were grown for an additional 20 h at 22 °C. The cells were then harvested by centrifugation at 5,000 \times g for 20 min at 4 °C. SeMet-substituted AIMP3 (Δ C5,T42M/I70M/K96M) was expressed in M9 minimal medium supplemented with 50 mg/ml SeMet. Cell pellets were resuspended in ice-cold buffer A (50 mM Tris-HCl, pH 8.0, 5 mM β -mercaptoethanol) and disrupted by ultrasonication. These crude cell extracts were then centrifuged at 11,000 \times g for 1 h at 4 °C. Cell lysates containing His₆-tagged AIMP3 were then bound to nickel-nitrilotriacetic acid-agarose (Qiagen) equilibrated with buffer A. After washing with buffer A containing 10 mM imidazole, bound proteins were eluted with buffer A containing 300 mM imidazole. The His₆ tag was then removed from AIMP3 by incubating with recombinant tobacco etch virus protease (Invitrogen), followed by nickel-nitrilotriacetic acid-agarose and ion exchange chromatography with HiTrap Q Sepharose (GE Healthcare). AIMP3 proteins contained two additional residues (Gly–Ala) at the N terminus because of the cloning procedure. Final protein yields were ~8–10 mg/liter, as determined by the Bradford procedure (Bio-Rad). Protein homogeneity was assessed by 10% SDS-PAGE and Coomassie Blue staining. The purified AIMP3 was then dialyzed against 50 mM Tris-HCl, pH 8.0, containing 300 mM NaCl; concentrated to 15 mg/ml; and stored at –80 °C.

Crystallization, Data Collection, and Structure Determination—AIMP3 proteins were concentrated and subjected to initial crystallization screening at 293 K using a sitting drop-vapor diffusion method with commercially available crystal-screening solution sets from Hampton Research and Emerald Biosystems. Full-length AIMP3 crystals were obtained using 0.1 M sodium cacodylate buffer, pH 6.5, containing 30% polyethylene glycol 8000 and 0.2 M sodium acetate. In the case of the deletion mutant protein, after optimization, the best crystals were obtained under the condition of 15% polyethylene glycol 10,000 in 0.1 M HEPES at pH 5.5. However, none of crystals diffracted well. Finally, the SeMet-substituted AIMP3 deletion mutant protein (human AIMP3 Δ C5,T42M/I70M/K96M) was subjected to crystallization screening. Crystallization conditions were optimized as 4% benzamidine HCl and 10% polyethylene glycol 10,000 in 0.1 M HEPES buffer at pH 7.0 with 2 μ l of 15 mg/ml protein and 2 μ l of the reservoir solution at 16 °C. Crystals appeared within 2 days and grew for about 5 days to reach maximal dimensions of ~0.1 \times 0.1 \times 0.1 mm.

A single crystal was transferred to the reservoir solution containing 20% glycerol as a cryoprotectant prior to x-ray data collection. Single wavelength anomalous dispersion data were collected at 0.9795 Å, the wavelength corresponding to the

selenium absorption peak, using an ADSC Quantum 210 CCD area detector at beamline 6C1 (MXW) at the Pohang Accelerator Laboratory. The completeness of the data collected was 98.3% at a resolution of 2.5 Å. This crystal was also used for data collection at a wavelength of 1.2399 Å, which produced the highest photon flux that could be obtained at beamline. Using a longer exposure time, diffraction data were collected at a higher resolution (2.0 Å). Data were integrated and scaled using the HKL2000 suite (15). The crystal belonged to the C222₁ space group with unit cell parameters of 46.3 \times 77.9 \times 194.8 Å. Six of the selenium atoms in the asymmetric unit were found using SOLVE (16). The asymmetric unit contained two molecules, and the value of the Matthew's coefficient was 2.25 Å³/Da, corresponding to a solvent content of 45.3%. The overall figure of merit was 0.347. Density modification and subsequent automated model building were done using RESOLVE (17), which increased the figure of merit to 0.694 with 76% (259 amino acid residues) of the residues incorporated. Further model building was performed manually into a density-modified electron density map using the program O (18) and Coot (19), and refinement with isotropic displacement parameters was performed using CCP4 remlac5 (20). In the final model, a loop region (Gly⁸⁴–Lys⁸⁸) in both AIMP3 molecules was not unassigned because electron density was poor in this region. The *R*_{work} and *R*_{free} values of the refined structure are 0.204 and 0.245, respectively. Crystallographic data statistics are summarized in supplemental Table 1. The final model has been deposited in the Protein Data Bank (21) under code 2UZ8.

Determination and Generation of AIMP3 Mutations—Bone marrow cells of chronic myeloid leukemia patients were obtained from the Korean Leukemia Cell and Gene Bank. Total RNAs were isolated from the cells of each patient using RNeasy (Qiagen) and subjected to reverse transcription-PCR to generate the AIMP3 cDNAs. These were then subcloned into the pcDNA3.1/His-TOPO vector (Invitrogen), and mutations were determined by DNA sequencing. Point mutations in AIMP3 were generated via site-directed mutagenesis using a QuikChange kit (Stratagene). All generated mutants were confirmed by DNA sequencing.

GST Pulldown Assay—Wild-type AIMP3 and mutants were synthesized by *in vitro* translation in the presence of [³⁵S]methionine using a coupled translation kit (TNT, Promega). MRS (900 amino acids full-length) and the 641-amino acid FAT domain of ATM were expressed as GST fusion proteins. Aliquots (10 μ l) of TNT products were incubated with 5 μ g of GST fusion proteins immobilized on glutathione-Sepharose 4B in 500 μ l of phosphate-buffered saline containing 0.5% Triton X-100, 0.5 mM EDTA, and 0.5 mM phenylmethylsulfonyl fluoride. The beads were incubated for 2 h at 4 °C with rotation and washed three times with phosphate-buffered saline buffer. After addition of SDS sample buffer, the bound proteins were eluted by boiling, separated by SDS-PAGE, and determined by autoradiography.

Coimmunoprecipitation—Myc-tagged wild-type AIMP3 and mutants were transfected into 293 cells with the FLAG-tagged FAT domain of ATM. The cells were UV light-irradiated at 50 J/m², harvested 15 min after irradiation, and lysed. FLAG-ATM was immunoprecipitated with anti-FLAG antibody, and co-

Three-dimensional Structure and Interaction of AIMP3/p18

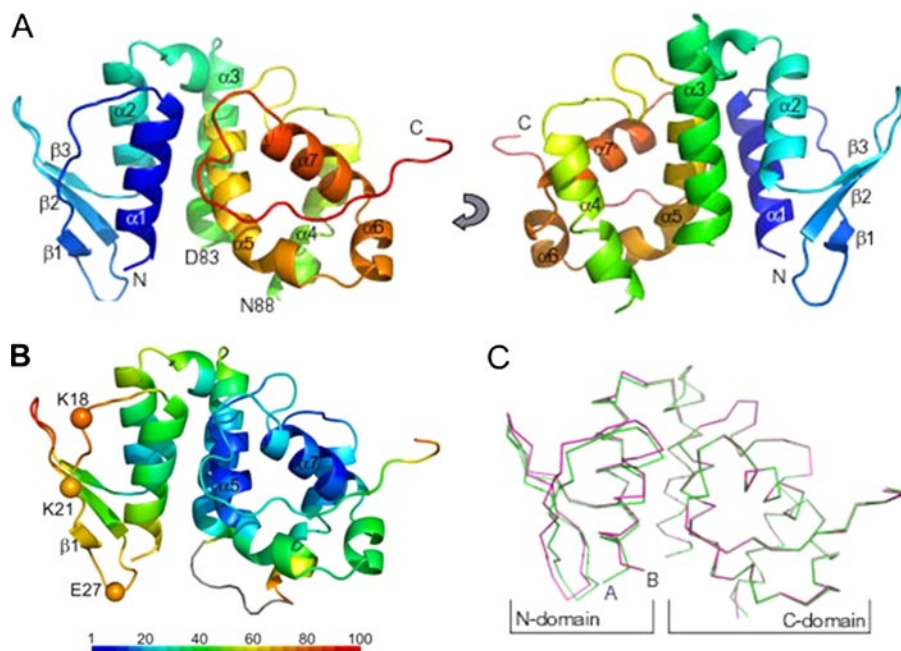


FIGURE 1. Structural characteristics of human AIMP3. *A*, ribbon diagrams of AIMP3 representing two domains. The N-terminal domain consists of a three-stranded antiparallel β sheet and two α helices, and the C-terminal domain contains five α helices with a long coiled structure at the C terminus. Residues 84–88 are missing. The left image is rotated by 180° in the y axis. Figures were generated using the PyMol program. *B*, *B*-factor representation by colors. The β sheet at the N-terminal domain has a higher *B*-factor (orange), and helices α 5 and α 7 form a stable core (blue) at the C-terminal domain. The missing loop region connecting helices α 3 and α 4 is lined in gray. Three residues with undefined side chains are shown as spheres. *C*, superimposition of two AIMP3 molecules (magenta and green) in an asymmetric unit. Relative positions of the N-terminal domain against the C-terminal domain from two molecules are slightly different from each other.

precipitation of Myc-AIMP3 was detected by immunoblotting with anti-Myc antibody.

Luciferase Reporter Gene Assay—HCT116 p53^{+/-} cells were grown in RPMI 1640 medium (HyClone) supplemented with 10% fetal bovine serum and penicillin/streptomycin. Each of the plasmids encoding the wild-type and mutant AIMP3 was transfected with p53-responsive p21 luciferase (kind gift of S. J. Um, Sejong University), and the β -galactosidase plasmids were transfected by electroporation using a Microporator-mini (Digital Bio Technology). Preparation of cell extracts and β -galactosidase and luciferase assays were performed according to the manufacturer's protocol (Promega). The values are the averages of at least two separate experiments and were normalized to those of β -galactosidase resulting from the expression of the internal control plasmid pCMV β gal.

RESULTS

Overall Structure—The three-dimensional structure of human AIMP3 was determined by x-ray crystallography using single wavelength anomalous dispersion and refined to a crystallographic *R*-factor of 0.204 at 2.0-Å resolution. The details of data collection and refinement statistics are summarized in supplemental Table 1. Two AIMP3 molecules (A and B) were found to be present in the asymmetric crystal unit and to be related by a non-crystallographic 2-fold axis of symmetry. AIMP3 consists of seven α helices and three β strands and is divided into two structural domains (Fig. 1A). The N-terminal domain (AIMP3-N) spanning Met¹–Asn⁵⁶ contains two α helices (α 1 and α 2) and three β strands. The three-stranded anti-

parallel β sheets are inserted between the two helices facing the same side of the β sheet. The β sheet was flanked by the parallel helices α 1 and α 2 on one side and exposed to solvent on the other side. The linker of 7 residues (Lys⁵⁷–Ser⁶³), in which the peptide from Glu⁵⁸ to Leu⁶¹ forms a 3_{10} helix, connects the two domains. A short-turn helix is also found in the linker connecting two domains in the structures of GSTs from maize (22) and mosquito (23). The C-terminal domain (AIMP3-C) consists of a bundle of five helices (α 3 to α 7) (Thr⁶⁴–Tyr¹⁵²) and a following coiled region (Pro¹⁵³–Leu¹⁶⁹). Two helices (α 3 and α 5) of the helical domain face the helices of AIMP3-N, forming a four-helix bundle-like structure. There are hydrophobic interactions between Leu¹⁰, Leu¹⁴, Val⁵², Leu⁷⁵, Ile¹¹⁸, and Leu¹¹⁹ of the two domains that stabilize the structure with an additional ion interaction (Glu⁶ from helix α 1 and Arg⁷⁸ from helix α 3). Helix α 5, which runs anti-

parallel to helix α 4 and parallel to helix α 3, bends away from AIMP3-N at its C-terminal end. Residues from Gly⁸⁴ to Lys⁸⁸ between helices α 3 and α 4 were not defined because of poor electron density in both molecules A and B, suggesting a flexible loop connecting the two helices. Average *B*-factors of molecules A and B are 31.7 and 33.4 Å², respectively. In both molecules, the *B*-factor of AIMP3-N is higher than that of AIMP3-C, which contains stable inter-helix interactions, suggesting a possible movement in the N-terminal domain (Fig. 1B). Specifically, *B*-factors at loops connecting β strands are high. Side chains of Lys¹⁸, Lys²¹, and Glu²⁷ in the loops are missing in both molecules. Two AIMP3 molecules in an asymmetric unit have essentially the same conformation. The root mean square deviation of main chain atoms between two molecules is 0.651 Å. However, the superimposed two molecules show a small difference in the relative position of AIMP3-N to AIMP3-C (Fig. 1C), implying a potential inter-domain movement.

Structural Similarity—A search using the DALI program (24) yielded several proteins structurally similar to AIMP3, including GSTs and other proteins with a GST fold (supplemental Table 2). *E. coli* GST (25) has the greatest Z-score (14.1), and other proteins including yeast elongation factor EF1B γ (26), prostaglandin D synthase (27), yeast prion protein Ure2p (28), *E. coli* stringent starvation A (29), and N-terminal domains from yeast Arc1p and glutamyl-tRNA synthetase (ERS) show Z-scores ranging from 9.9 to 13.9 (30). Arc1p forms a trimeric complex with ERS and MRS in yeast (31). All proteins except Arc1p have a similar two-domain structure like GST, whereas Arc1p lacks a motif corresponding to the N-terminal

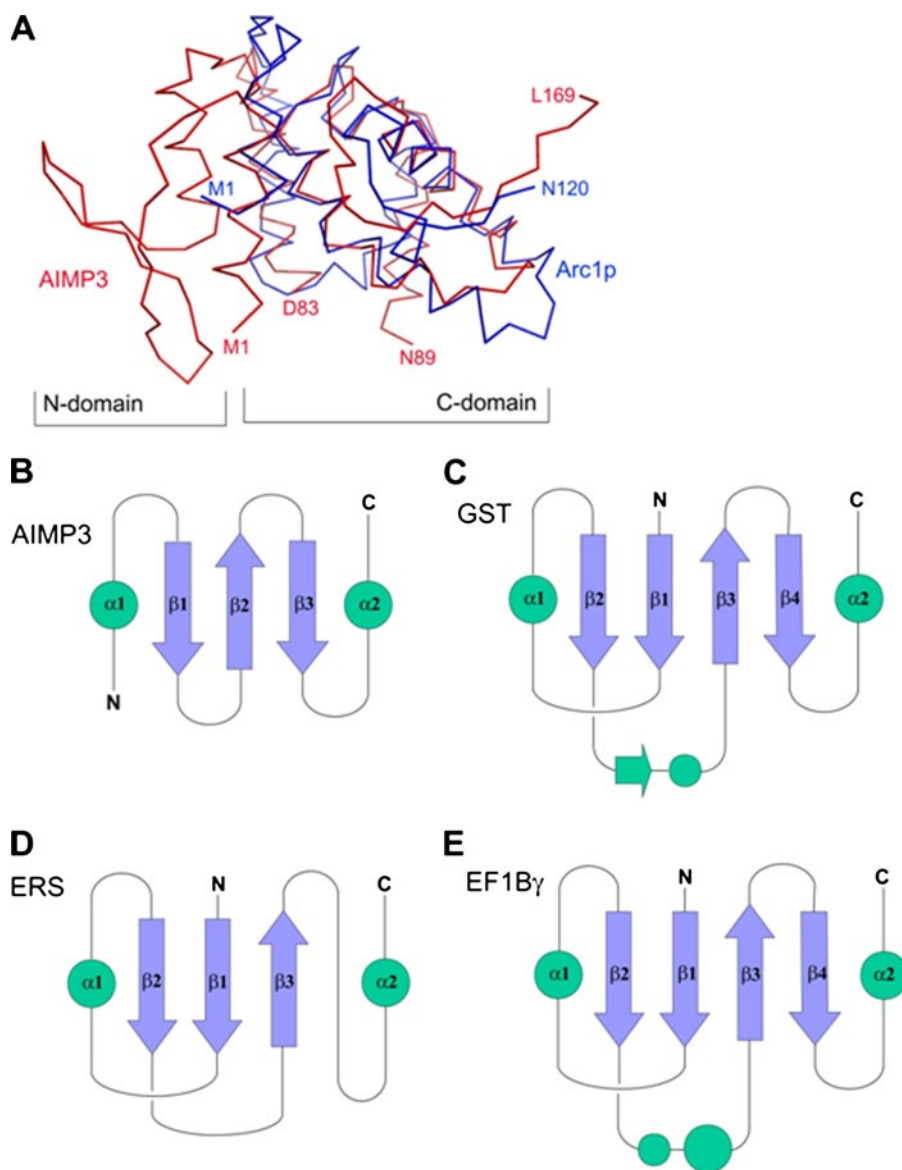


FIGURE 2. **Structural comparison of AIMP3 with other proteins with GST homology domains.** A, superimposition of yeast Arc1p on AIMP3. AIMP3 (red) has a C-terminal domain similar to Arc1p (blue). Topology diagrams of AIMP3-N (B), *E. coli* GST (C), yeast ERS (D), and EF1B γ (E) are shown. AIMP3 and ERS have a three-stranded β sheet, whereas GST and EF1B γ have a four-stranded β sheet. Although AIMP3 contains an antiparallel β sheet, the other three proteins have a β strand at the N terminus, forming a mixed β sheet. Additional secondary structures in the long loop between $\beta 2$ and $\beta 3$ strands are present in GST and EF1B γ .

domain of GST. The conformation of the Arc1p N-terminal domain is similar to AIMP3, though it does not possess the N-terminal β sheet and $\alpha 2$ helix of AIMP3 (Fig. 2A). Arc1p has an α helix ahead of the helical domain, which corresponds to the C-terminal domain of GST, and this first helix is apart from the second helix and is located near the fourth helix-like helix $\alpha 1$ in AIMP3-N. It also has a similar linker region containing a 3_{10} helix between the first helix and the helical domain.

AIMP3-N possesses a three-stranded antiparallel β sheet with a strand order of 1-2-3 (Fig. 2B), whereas GST and other structurally related proteins contain a four-stranded mixed β sheet in their N-terminal domains. Furthermore, GST has a β strand at its N terminus that is inserted between the $\beta 2$ and $\beta 3$ strands, forming a strand order of 2-1-3-4 (Fig. 2C). Although ERS has a three-stranded β sheet, it has a long loop connecting

the $\beta 3$ strand and $\alpha 2$ helix in the position corresponding to the $\beta 4$ strand of GST, implying a dissolved fourth β strand (Fig. 2D). A short $\beta 1$ - $\beta 2$ loop makes AIMP3-N smaller than other proteins. *E. coli* GST contains an additional strand and α helix in the $\beta 2$ - $\beta 3$ loop corresponding to the $\beta 1$ - $\beta 2$ loop of AIMP3 (Fig. 2C). EF1B γ contains an extra helix and turn in that loop (Fig. 2E). These differences in the presence of an underlying overall similarity imply that these proteins might have their unique functions.

Although overall folding of the C-terminal α helical domains of AIMP3 and related proteins is similar, the length of the helices and conformation of the C-terminal tails show difference. AIMP3-C shows more similarity to C-terminal domains of ERS and Arc1p than to those of GST or EF1B γ , which have longer $\alpha 3$ and $\alpha 4$ helices. Arc1p has a shorter $\alpha 4$ helix and $\alpha 3$ - $\alpha 4$ loop, whereas ERS has a helical C-terminal tail. Despite that overall amino acid sequence homologies between these proteins are low (13–23% identity), there are discernible sequence similarities in the core region of helical domain and motifs like helices $\alpha 3$ and $\alpha 7$. For example, the sequence of AIMP3 helix $\alpha 7$ (VNVSRWYTL) is similar to that of the ERS helix (LNVSRWFCH) with the conserved Arg¹⁴⁴ of AIMP3, Arg¹⁶⁴ of ERS, Arg¹⁹⁰ of EF1B γ , and Arg¹⁰⁰ of Arc1p.

Putative Binding Sites—Crystallographic inspection suggests that AIMP3 can make two types of inter-

actions. In an asymmetric unit, two molecules, A and B, are arranged by a non-crystallographic 2-fold axis (Fig. 3A). Helix $\alpha 7$ and the loop between helices $\alpha 4$ and $\alpha 5$ are involved in the interaction. The other interaction type is dimer formation by a crystallographic 2-fold axis (Fig. 3B). Helices $\alpha 2$ and $\alpha 3$ from both monomers are arranged to form a four-helix bundle, and helix $\alpha 3$ of one monomer binds to the interface between the $\beta 3$ strand and $\alpha 2$ helix of the other monomer. Two different topologically identical dimers, *i.e.* AA and BB, could be formed by a crystallographic axis. Side chains of Gln⁷³ and Glu⁷⁶ from helix $\alpha 3$ have hydrogen bonds with the hydroxyl groups of Thr⁴⁵ and Thr⁴⁶ from helix $\alpha 2$ and the main chain nitrogen of Thr⁴² of another monomer. There are additional interactions between the guanidine group of Arg²⁸ and the main chain oxygen atoms of Thr⁸⁰ and Asp⁸³.

Three-dimensional Structure and Interaction of AIMP3/p18

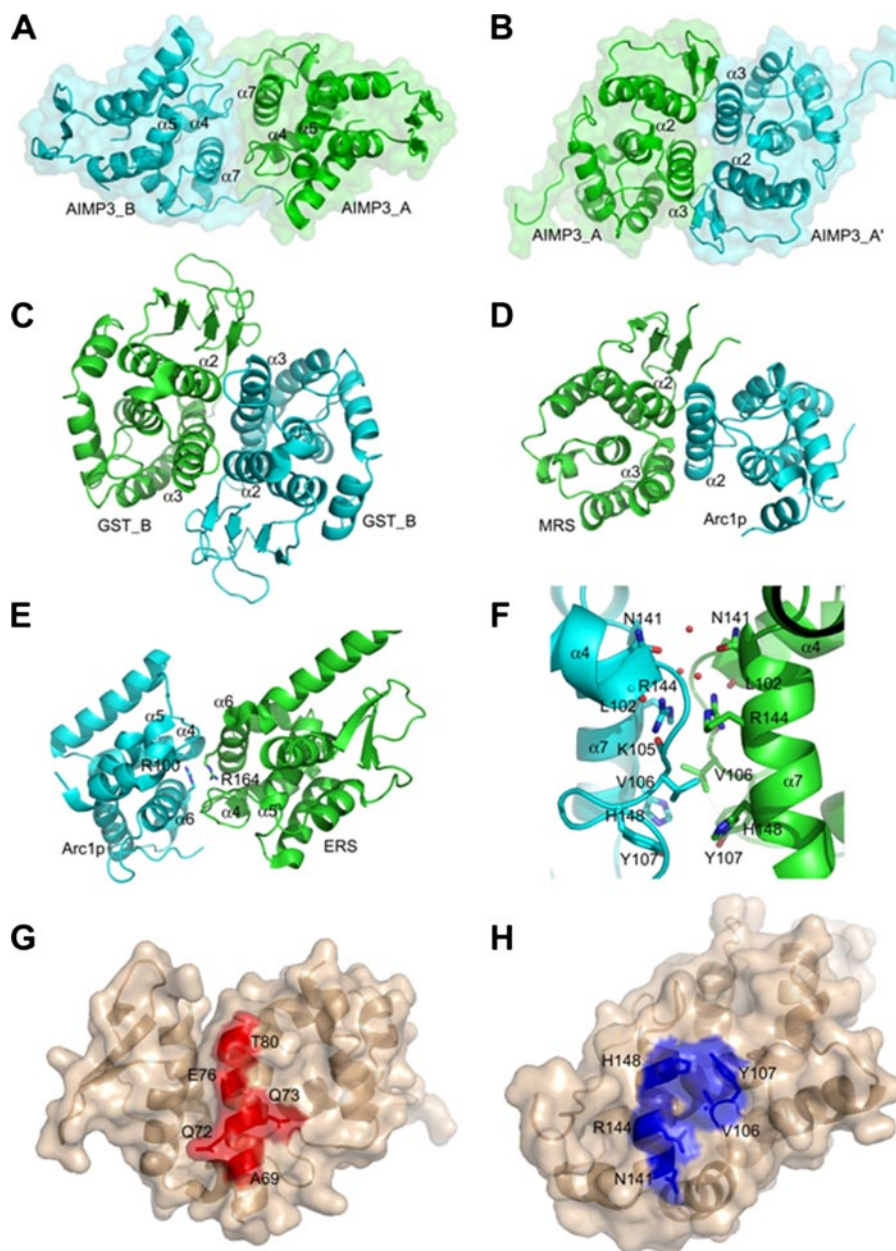


FIGURE 3. Prediction of putative molecular interaction sites. *A*, interaction between two AIMP3 molecules in the asymmetric crystal unit. *B*, dimer formation between two AIMP3 molecules with crystallographic 2-fold symmetry. *C*, dimeric interaction of *E. coli* GST. *D*, interaction between the N-terminal domains of yeast Arc1p and MRS. *E*, interaction between the N-terminal domains of yeast Arc1p and ERS. *F*, interactions between the residues in the $\alpha 7$ helices of two AIMP3 molecules in the asymmetric unit. Side chains of Val¹⁰⁶, Tyr¹⁰⁷, Asn¹⁴¹, Arg¹⁴⁴, and His¹⁴⁸ and carbonyl groups of Leu¹⁰² and Lys¹⁰⁵ are shown as sticks. Water molecules mediating hydrogen bonds between two AIMP3 are shown as red spheres. *G* and *H*, surface contour and residues of AIMP3 are located at putative binding sites I and II, respectively.

The interaction between the two AIMP3 molecules related to the crystallographic 2-fold axis is similar to that shown by the GST dimer, in which interactions occur around helix $\alpha 3$ (Fig. 3C). The GST-like domain of EF1B γ mediates the dimerization of the EF1 complex, which in yeast is a dimer of the heterotrimer EF1A/EF1B α /EF1B γ . Residues from both the N-terminal thioredoxin fold and C-terminal α helical domain of EF1B γ form the dimer interface. In the trimeric complex of yeast Arc1p with ERS and MRS (32), the N-terminal domains of Arc1p and MRS form a complex similar to the homodimers of GST and AIMP3 (Fig. 3D). Together with sequence homology

at helix $\alpha 3$, the area around Ala⁶⁹, Glu⁷², Gln⁷³, Glu⁷⁶, and Thr⁸⁰ from helix $\alpha 3$ is thought to constitute a putative binding site for the molecular interaction of AIMP3 (putative binding site I) (Fig. 3G).

The interaction between ERS and Arc1p includes interactions along their $\alpha 6$ helices, which correspond to helix $\alpha 7$ of AIMP3 (Fig. 3E). The stacking of Arg¹⁶⁴ from ERS and Arg¹⁰⁰ from Arc1p makes their key interaction, and the interface of the two proteins exhibits a large number of inter-atomic interactions (32). This interaction shows the “lock and key” complementary features of a hydrophobic surface with a limited number of the electrostatic interactions. It is similar to the interaction of two AIMP3 molecules in an asymmetric unit involving a region of helix $\alpha 7$ and a loop between helices $\alpha 4$ and $\alpha 5$. As aforementioned, the sequence of AIMP3 helix $\alpha 7$ is well conserved in the corresponding helix of ERS. Arg¹⁴⁴ residues from the $\alpha 7$ helices of two AIMP3 molecules are stacked on each other and have a hydrogen bond network through water molecules with the main chain carbonyl oxygen of Glu¹⁰³ of the other AIMP3 (Fig. 3F). Asn¹⁴¹ also shows water-mediated hydrogen bonds with Asn¹⁴¹ and Glu¹⁰³ of the other molecule, whereas Val¹⁰⁶, Tyr¹⁰⁷, and His¹⁴⁸ from both monomers are in close proximity. Based on this structural feature and sequence homology, this interaction is predicted to provide another putative binding site for AIMP3 (putative binding site II) (Fig. 3H).

Mutagenesis—We also investigated the functions of AIMP3 residues that are important for its interaction with ATM because the binding of these two proteins is critical for the tumor-suppressive activity of AIMP3. It has been reported that AIMP3-heterozygous mice develop various cancers including lymphoma at high frequency and, furthermore, that the allelic deletion of AIMP3 is often observed in cancer patients including leukemia patients (8). To identify mutations affecting the interaction of AIMP3 with ATM, we isolated the gene encoding AIMP3 from 20 different chronic myeloid leukemia (CML) patients. Fourteen of these cases contained mutations at the different residues of AIMP3 (supplemental Table 3), and of these mutations, Glu⁷⁶/Thr⁸⁰ and Val¹⁰⁶/Arg¹⁴⁴ are

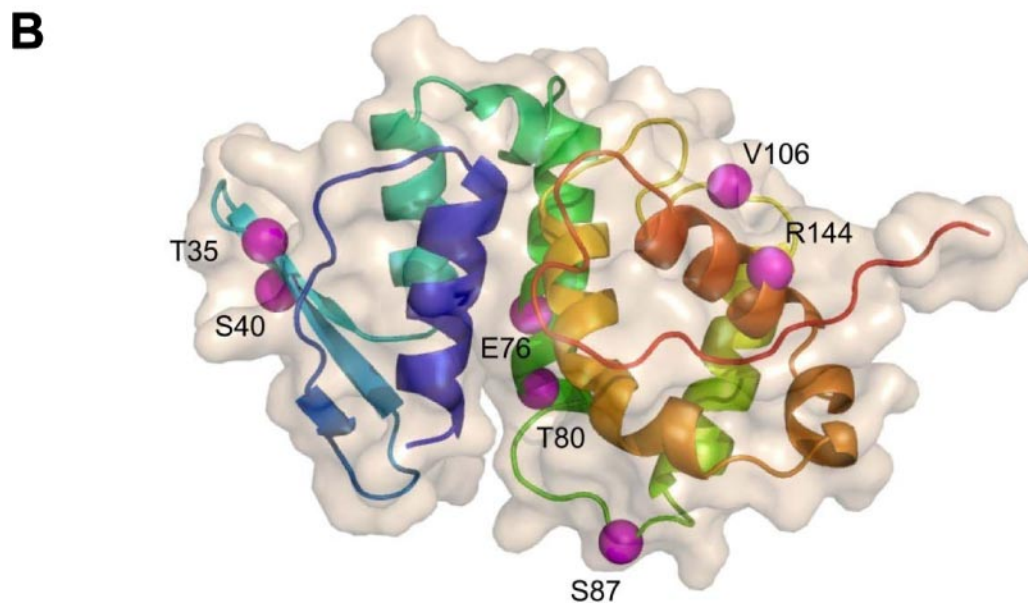
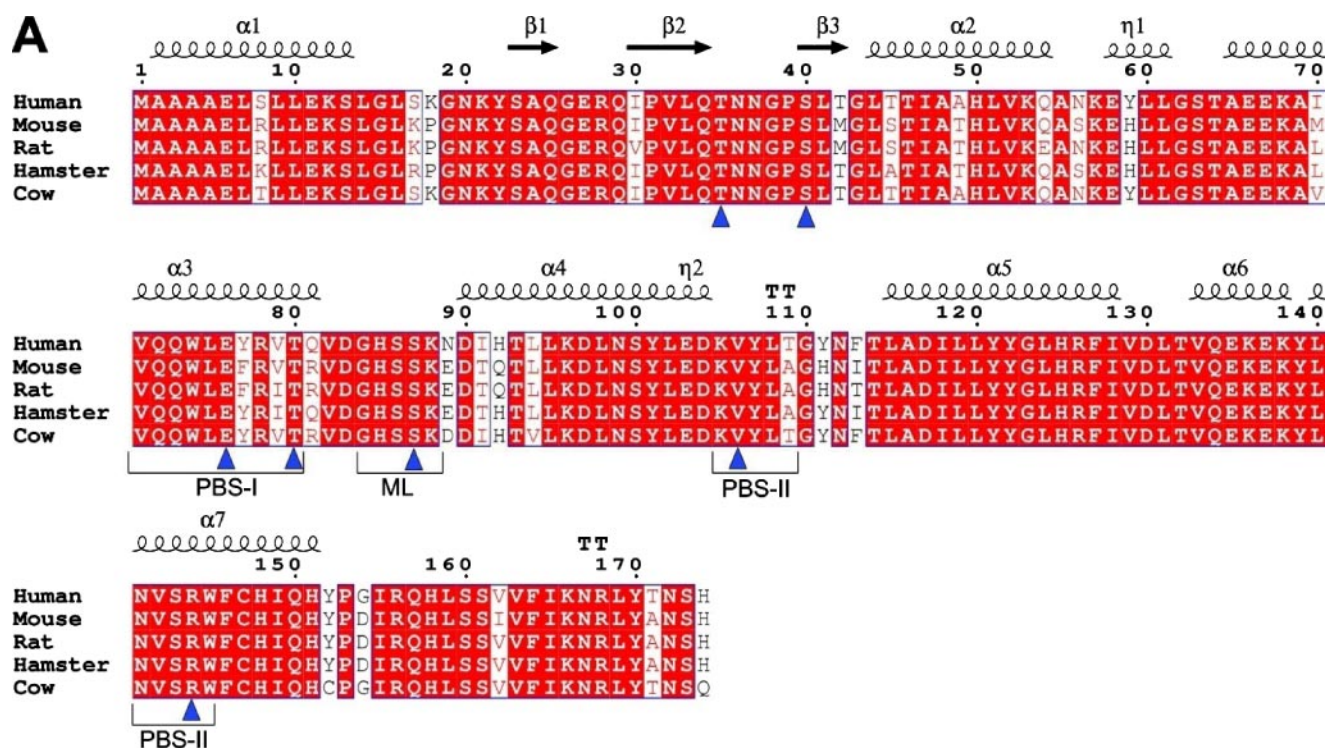


FIGURE 4. Locations of AIMP3 mutations found in CML patients. *A*, sequence alignment of AIMP3 from human (NP_004271), cow (NP_001035689), hamster (P70102), mouse (NP_079656), and rat (XP_214451). The alignments shown represent secondary structures of human AIMP3. Conserved residues are set against a red background. Mutated residues in AIMP3 identified from CML patients are marked with arrowheads. Putative binding sites (PBS) I and II and a missing loop (ML) are indicated. Multiple alignment was done using the T-coffee software and visualized using ESPript. TT, tight turn. *B*, spatial locations of AIMP3 mutations isolated from leukemia patients. Mutated residues Thr³⁵ and Ser⁴⁰ are located in the N-terminal domain; Val¹⁰⁶, Arg¹⁴¹, and Arg¹⁴⁴ are located in the C-terminal domain; and Glu⁷⁶, Thr⁸⁰, and Ser⁸⁷ are located in the loop connecting the β3 and β4 strands.

located at putative binding sites I and II, respectively (Fig. 4, *A* and *B*). Moreover, Ser⁸⁷ resides in the loop between helices α3 and α4, and Thr³⁵ and Ser⁴⁰ are in the extruding β hairpin consisting of β2 and β3 strands. The side chain of Thr³⁵ faces the helix α2, whereas the Ser⁴⁰ side chain is exposed to solvent (Fig. 4, *A* and *B*).

Effect of Mutation on ATM Binding and p53 Activation—We introduced alanine substitutions to the residues of AIMP3 (Thr³⁵/Ser⁴⁰, Thr⁷⁶, Thr⁸⁰, Ser⁸⁷, Val¹⁰⁶, and Arg¹⁴⁴) whose

mutations have been identified in CML patients and examined whether any of these mutations affect its interactions with ATM and MRS using *in vitro* pulldown and coimmunoprecipitation assays. ATM is a 3056-amino acid kinase that is involved in cell cycle control and DNA repair and consists of FAT (FRAP/ATM/TRRAF conserved), phosphatidylinositol 3-kinase catalytic, and C-terminal domains. Here we used the 641-amino acid FAT domain of ATM, which was shown previously to be involved in its interaction with AIMP3 (33), and full-

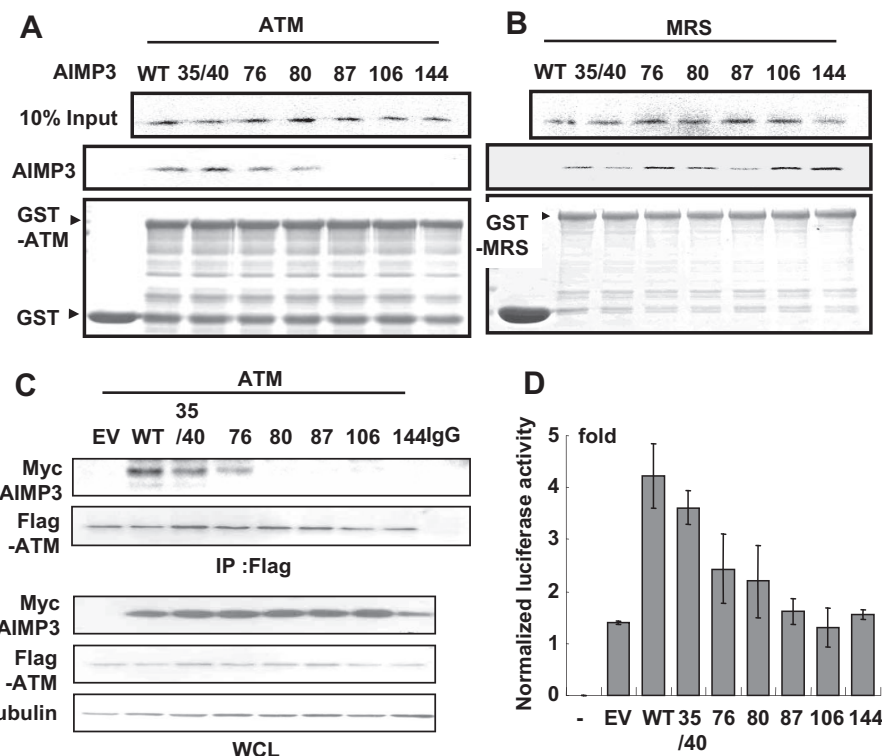


FIGURE 5. Effect of mutations of AIMP3 on its interaction with ATM and p53 activation. *A* and *B*, radioactive human wild-type (WT) AIMP3 and mutants were synthesized by *in vitro* translation and mixed with the FAT domain of human ATM (*A*) or with full-length MRS (*B*) expressed as a GST fusion protein. GST proteins were precipitated with glutathione-Sepharose, and coprecipitation of AIMP3 was determined by autoradiography. *C*, Myc-AIMP3 and FLAG-ATM were coexpressed in 293 cells. After UV irradiation, cells were lysed and immunoprecipitated (IP) with anti-FLAG antibody, and coprecipitation of Myc-AIMP3 was determined by immunoblotting with anti-Myc antibody. WCL, whole cell lysates; EV, empty vector. *D*, HCT116 p53^{+/-} cells were transfected with p21-dependent luciferase and wild-type AIMP3 or the individual mutants. Cells were irradiated with UV light at 50 J/m² and incubated for 2 h. They were then lysed, and luciferase activities were measured and normalized by the β -galactosidase activity that was cotransfected with luciferase. Experiments were performed in triplicate and repeated twice. Averaged values are shown in the bar graph.

length MRS. Wild-type AIMP3 and mutants were prepared by *in vitro* translation in the presence of ³⁵S and mixed with the FAT domain of ATM or MRS expressed as a GST fusion protein. GST proteins were precipitated using glutathione-Sepharose, and the coprecipitation of AIMP3 mutants was followed by autoradiography. It was found that mutants at Thr³⁵/Ser⁴⁰, Glu⁷⁶, and Thr⁸⁰ coprecipitated with ATM-like wild-type AIMP3 but that S87A, V106A, and R144A mutants lost their ATM binding ability (Fig. 5A). However, all of these mutants still retained their ability to bind MRS (Fig. 5B), suggesting that AIMP3 may associate with the two target proteins in different manners or affinities. We also checked the effect of these mutations on the cellular interaction between AIMP3 and ATM by coimmunoprecipitation. Myc-tagged wild-type AIMP3 or mutants were coexpressed with FLAG-ATM in 293 cells, which were then subjected to UV irradiation. FLAG-ATM was immunoprecipitated with anti-FLAG antibody, and coprecipitated AIMP3 mutants were determined by immunoblotting with anti-Myc antibody. All of the mutants except for R144A were expressed to a level comparable with that of wild-type AIMP3, suggesting that these mutations did not affect the cellular stability of AIMP3 (Fig. 5C, lower panel). However, the expression of the R144A mutant was significantly lower compared with others after transfecting the same amount of the plasmid, which

implied that this mutation had destabilized the protein structure (data not shown). In this assay, the T80A, S87A, V106A, and R144A mutants were not coprecipitated with ATM (Fig. 5C). Although loss of interaction for Ser⁸⁷, Val¹⁰⁶, and Arg¹⁴⁴ mutants had already been demonstrated by the pull-down assay above, the T80A mutant was newly identified to be defective in terms of ATM binding by coimmunoprecipitation. At this moment, it is not clear why the T80A mutant cannot bind ATM in the cells while retaining its ATM binding ability *in vitro*. Perhaps, it is defective in nuclear localization, which is required for the interaction with ATM or in dissociation from MRS. Our combined findings concerning predicted putative binding sites and the effects of mutation on ATM binding suggest that putative binding site II, which includes Val¹⁰⁶ and Arg¹⁴⁴, is likely to be involved in the interaction with ATM.

We then introduced the wild-type AIMP3 and mutants into HCT116 cells harboring the luciferase reporter under the p21 promoter and irradiated transfectants with UV light. Although transfection of wild-type AIMP3 enhanced the luciferase activity about 4-fold, all mutants except for the Thr³⁵/Ser⁴⁰ mutant demonstrated less luciferase activity than the wild type (Fig. 5D). In this assay, the three mutations at Ser⁸⁷, Val¹⁰⁶, and Arg¹⁴⁴ that blocked the interaction of AIMP3 with ATM most dramatically reduced the luciferase activity, which suggests that these residues are functionally important for p53 activation and ATM interaction.

DISCUSSION

The multi-ARS complex harbors many multifunctional enzymes and associated factors and is considered a molecular depot or signalosome (1, 34). Thus, it is important to understand the molecular assembly and dynamic status of its components to comprehend how the multitasking of this complex is regulated. The complex consists of nine different ARSs and three AIMP3s. Among these components, GST homology domains are found in the N-terminal appendices of two ARSs (MRS and glutamylprolyl-tRNA synthetase) and two AIMP3s (AIMP2 and AIMP3) (35). Because these domains are detected only in these complex-forming ARSs and AIMP3s and in the N-terminal appendix of valyl-tRNA synthetase that also forms a complex with the elongation factor (36), they are thought to be critical for the assembly of protein complexes. In fact, we observed that the N-terminal appendix of MRS, which contains

a GST homology domain, interacts with AIMP3 (data not shown), further supporting this notion. In this interaction pair, AIMP3 is required for the cellular stability of MRS but does not need MRS for its own stability (37). Another target protein of AIMP3, ATM, does not contain a GST homology domain, suggesting that AIMP3 may associate with ATM in a different manner. In fact, mutations of AIMP3 that abolished the interaction with ATM did not influence its binding to MRS (Fig. 5, A and B). Although AIMP3 is necessary for the stability of MRS, it also functions as a positive regulator of the kinase activity of ATM (8). In addition, AIMP3 could target itself to form a homodimer, as implied by crystal packing shown in the present study and by previous yeast two-hybrid analyses (38). Nonetheless, gel filtration analysis of the purified AIMP3 showed no solid evidence of homodimer in solution (data not shown).

We found previously that AIMP3 is translocated into the nucleus in the presence of DNA damage (8) or oncogenic stress (9). Because its nuclear translocation occurs within 15 min of UV irradiation, it does not appear to involve *de novo* synthesis. Instead, AIMP3 bound to the multi-ARS complex could dissociate from the complex and subsequently translocate to the nucleus. If this is the case, the binding of AIMP3 to its two target proteins, MRS and ATM, might be controlled by post-translational modification. In this regard, it should be noted that glutamylprolyl-tRNA synthetase, the largest component of the multi-ARS complex, is phosphorylated and dissociates from the complex after interferon- γ treatment to form some different type of multi-protein complex that is required for gene silencing (39). Thus, it is possible that AIMP3 binding and movement could also be controlled by phosphorylation or some other post-translational modification.

Among the three residues that abrogated ATM binding ability, Val¹⁰⁶ and Arg¹⁴⁴ are located in putative binding site II (Fig. 4) and thus are expected to be involved in the interaction with ATM. However, Ser⁸⁷ is unlikely to be directly involved in the binding to ATM because it is rather remote from putative binding site II and faces the other side (Fig. 4). Perhaps, Ser⁸⁷ is involved in post-translational modification or the disposition of the binding site for the interaction with ATM. On the other hand, mutation at Arg¹⁴⁴ not only abolished the ATM binding ability but also appeared to destabilize the protein folding (data not shown). For this reason, we had to transfect much larger amounts of the encoding plasmid to express this mutant to the level comparable with those of the wild type or other mutants. Because the two amino groups of the Arg¹⁴⁴ side chain form hydrogen bonds with the carbonyl oxygen of Leu¹⁰² and Lys¹⁰⁵ to stabilize the interaction between helices $\alpha 4$ and $\alpha 7$ (Fig. 3F), loss of this residue might result in the unfolding of the C-terminal domain. At present, it is unclear why the mutants beyond binding site II reduced the ability of AIMP3 to activate p53 (Fig. 5D). Perhaps, they can still bind but not efficiently activate ATM or indirectly influence the conformation of the ATM binding site in AIMP3.

Because AIMP3 exerts its tumor-suppressive activity by binding ATM, any mutation that affects their binding is likely to be etiologically associated with cancer formation. In the present study, we identified several mutations of AIMP3 isolated from clinical specimens of CML patients. CML is a neo-

plastic disease of hematopoietic stem cells and is caused by the expression of abnormally fused BCR/ABL tyrosine kinase. This oncogenic kinase is encoded by the Philadelphia chromosome that results from the translocation between chromosomes 9 and 22, which harbor the *c-abl* and *bcr* genes, respectively. Although its molecular pathogenesis is relatively well known compared with those of other cancers, additional mutations at other critical genes could be associated with disease progression or drug resistance. At present, we do not know whether these mutants have any pathological implications for CML. Nevertheless, because AIMP3 is critical for the stability of chromosome structure (9), mutations affecting AIMP3 activity could be associated with the initiation or progression of leukemia or other related cancers. Although these questions need further investigation, the presence of the mutations found in cancer patients, which affect the interaction of AIMP3 with ATM and its ability to activate p53, further supports the functional significance of AIMP3 in the control of tumorigenesis. Furthermore, the interface between AIMP3 and ATM identified from this work provides a new therapeutic window for the development of novel anti-cancer agents.

Acknowledgment—We thank Dr. Urszula Derewenda (University of Virginia) for kind advice concerning protein crystallization.

REFERENCES

1. Park, S. G., Ewalt, K. L., and Kim, S. (2005) *Trends Biochem. Sci.* **30**, 569–574
2. Ko, Y.-G., Park, H., Kim, T., Lee, J.-W., Park, S. G., Seol, W., Kim, J. E., Lee, W.-H., Kim, S.-H., Park, J. E., and Kim, S. (2001) *J. Biol. Chem.* **276**, 23028–23033
3. Kim, E., Kim, S.-H., Kim, S., and Kim, T. S. (2006) *J. Immunol.* **176**, 256–264
4. Park, S. G., Kang, Y.-S., Ahn, Y. H., Lee, S. H., Kim, K.-R., Kim, K.-W., Koh, G. Y., Ko, Y.-G., and Kim, S. (2002) *J. Biol. Chem.* **277**, 45243–45248
5. Park, S. G., Shin, H., Shin, Y. K., Lee, Y., Choi, E.-C., Park, B.-J., and Kim, S. (2005) *Am. J. Pathol.* **166**, 387–398
6. Park, S. G., Kang, Y.-S., Kim, J. Y., Lee, C. S., Ko, Y.-G., Lee, W. J., Lee, K. U., Yeom, Y. I., and Kim, S. (2006) *Proc. Natl. Acad. Sci. U. S. A.* **103**, 14913–14918
7. Kim, M. J., Park, B.-J., Kang, Y.-S., Kim, H. J., Park, J.-H., Kang, J. W., Lee, S. W., Han, J. M., Lee, H.-W., and Kim, S. (2003) *Nat. Genet.* **34**, 330–336
8. Park, B.-J., Kang, J. W., Lee, S. W., Choi, S. J., Shin, Y. K., Ahn, Y. H., Choi, Y. H., Choi, D., Lee, K. S., and Kim, S. (2005) *Cell* **120**, 209–221
9. Park, B.-J., Oh, Y. S., Park, S. Y., Choi, S. J., Rudolph, C., Schlegelberger, B., and Kim, S. (2006) *Cancer Res.* **66**, 6913–6918
10. Jeong, E. J., Hwang, G. S., Kim, K. H., Kim, M. J., Kim, S., and Kim, K. S. (2000) *Biochemistry* **39**, 15775–15782
11. Cahuzac, B., Berthonneau, E., Birlirakis, N., Guittet, E., and Mirande, M. (2000) *EMBO J.* **19**, 445–452
12. Cheong, H. K., Park, J. Y., Kim, E. H., Lee, C., Kim, S., Kim, Y., Choi, B. S., and Cheong, C. (2003) *Int. J. Biochem. Cell Biol.* **35**, 1548–1557
13. Kim, Y., Shin, J., Li, R., Cheong, C., Kim, K., and Kim, S. (2000) *J. Biol. Chem.* **275**, 27062–27068
14. Renault, L., Kerjan, P., Pasqualato, S., Menetrey, J., Robinson, J.-C., Kawaguchi, S., Vassilyev, D. G., Yokoyama, S., Mirande, M., and Cherfils, J. (2001) *EMBO J.* **20**, 570–578
15. Otwinowski, Z., and Minor, W. (1997) *Methods Enzymol.* **276**, 307–326
16. Terwilliger, T. C., and Berendzen, J. (1999) *Acta Crystallogr. Sect. D Biol. Crystallogr.* **55**, 849–861
17. Terwilliger, T. C. (2001) *Acta Crystallogr. Sect. D Biol. Crystallogr.* **57**, 1755–1762
18. Jones, T. A., Zou, J. Y., Cowan, S. W., and Kjeldgaard, M. (1991) *Acta*

Three-dimensional Structure and Interaction of AIMP3/p18

- Crystallogr. Sect. A* **47**, 110–119
19. Emsley, P., and Cowtan, K. (2004) *Acta Crystallogr. Sect. D Biol. Crystallogr.* **60**, 2126–2132
 20. Murshudov, G. N., Vagin, A. A., and Dodson, E. J. (1997) *Acta Crystallogr. Sect. D Biol. Crystallogr.* **53**, 240–255
 21. Berman, H. M., Westbrook, J., Feng, Z., Gilliland, G., Bhat, T. N., Weissig, H., Shindyalov, I. N., and Bourne, P. E. (2000) *Nucleic Acids Res.* **28**, 235–242
 22. Neufeind, T., Huber, R., Dasenbrock, H., Prade, L., and Bieseler, B. (1997) *J. Mol. Biol.* **274**, 446–453
 23. Oakley, A. J., Harnnoi, T., Udomsinprasert, R., Jirajaroenrat, K., Ketterman, A. J., and Wilce, M. C. (2001) *Protein Sci.* **10**, 2176–2185
 24. Holm, L., and Sander, C. (1993) *J. Mol. Biol.* **233**, 123–138
 25. Nishida, M., Harada, S., Noguchi, S., Satow, Y., Inoue, H., and Takahashi, K. (1998) *J. Mol. Biol.* **281**, 135–147
 26. Jeppesen, M. G., Ortiz, P., Shepard, W., Kinzy, T. G., Nyborg, J., and Andersen, G. R. (2003) *J. Biol. Chem.* **278**, 47190–47198
 27. Kanaoka, Y., Ago, H., Inagaki, E., Nanayama, T., Miyano, M., Kikuno, R., Fujii, Y., Eguchi, N., Toh, H., Urade, Y., and Hayaishi, O. (1997) *Cell* **90**, 1085–1095
 28. Umland, T. C., Taylor, K. L., Rhee, S., Wickner, R. B., and Davies, D. R. (2001) *Proc. Natl. Acad. Sci. U. S. A.* **98**, 1459–1464
 29. Hansen, A. M., Gu, Y., Li, M., Andrykovitch, M., Waugh, D. S., Jin, D. J., and Ji, X. (2005) *J. Biol. Chem.* **280**, 17380–17391
 30. Simader, H., Hothorn, M., and Suck, D. (2006) *Acta Crystallogr. Sect. D Biol. Crystallogr.* **62**, 1510–1519
 31. Simos, G., Segref, A., Fasiolo, F., Hellmuth, K., Shevchenko, A., Mann, M., and Hurt, E. C. (1996) *EMBO J.* **15**, 5437–5448
 32. Simader, H., Hothorn, M., Kohler, C., Basquin, J., Simos, G., and Suck, D. (2006) *Nucleic Acids Res.* **34**, 3968–3979
 33. Bosotti, R., Isacchi, A., and Sonnhammer, E. L. (2000) *Trends Biochem. Sci.* **25**, 225–227
 34. Ray, P. S., Arif, A., and Fox, P. L. (2007) *Trends Biochem. Sci.* **32**, 158–164
 35. Lee, S. W., Cho, B. H., Park, S. G., and Kim, S. (2004) *J. Cell Sci.* **117**, 3725–3734
 36. Negrutskii, B. S., Vyacheslav, F. S., Kerjan, P., El'skaya, A. V., and Mirande, M. (1999) *J. Biol. Chem.* **274**, 4545–4550
 37. Han, J. M., Lee, M. J., Park, S. G., Lee, S. H., Razin, E., Choi, E.-C., and Kim, S. (2006) *J. Biol. Chem.* **281**, 38663–38667
 38. Quevillon, S., Robinson, J.-C., Berthonneau, E., Siatecka, M., and Mirande, M. (1999) *J. Mol. Biol.* **285**, 183–195
 39. Sampath, P., Mazumder, B., Seshadri, V., Gerber, C. A., Chavatte, L., Kinter, M., Ting, S. M., Dignam, J. D., Kim, S., Driscoll, D. M., and Fox, P. L. (2004) *Cell* **119**, 195–208